The Effect of SiO_2 Addition to the Hydroxyapatite/Curcumin Composite Properties

Tri Windarti*, Nor Basid Adiwibawa Prasetya, and Ngadiwiyana Ngadiwiyana

Department of Chemistry, Faculty of Science and Mathematics, Universitas Diponegoro, Jl. Prof. Soedharto SH, Tembalang, Semarang 50275, Indonesia

Corresponding author:

email: tri.windarti@lecturer.undip.ac.id

Received: February 2, 2024
Accepted: June 11, 2024

DOI: 10.22146/ijc.93802

Abstract: *Hydroxyapatite/curcumin composites have been studied as a calcium phosphate cement candidate. In this research, the effects of adding SiO_2 to the hydroxyapatite/curcumin composite on the characteristics of the cement, such as the crystal and surface properties, as well as the release behavior of curcumin in Ringer's solution media, were studied. The composite preparation with and without SiO_2 was carried out using a Na_2HPO_4 2.5% solution. The results showed that the addition of 25% SiO_2 to the hydroxyapatite/curcumin composite did not change the crystal properties of hydroxyapatite but produced a more homogenous distribution of the ingredients. The behavior of the composite in Ringer's solution also changes, which is proven by the change in the crystal growth direction and Ca/P ratio. Adding SiO_2 produced a composite with a platter and larger particles, as well as a higher Ca/P ratio on the surface. The presence of SiO_2 inhibited the release of curcumin in which the ratio of HA: curcumin changed from 77.7%:22.3% to 69.6%:30.4% after 5 d of immersion in Ringer's solution. Thus, besides increasing calcium phosphate deposition on the cement surface, SiO_2 also prevents curcumin from being released from the composite.*

Keywords: *hydroxyapatite; curcumin; SiO_2; calcium phosphate cement*

■ INTRODUCTION

Under certain conditions, treatment of osteoporosis with antiresorptive drug therapy is ineffective due to the significant decrease in bone mineral density (BMD) [1]. Therefore, a bone filler can be applied to increase bone density. One bone filler material that has been developed for osteoporotic bone is calcium-based nanomaterial due to its similarities to natural bone minerals [2]. Among calcium-based nanomaterials, hydroxyapatite (HA, $Ca_{10}(PO_4)_6(OH)_2$) is known to have good biocompatibility and bioactivity properties [3-4]. Considering that oxidative stress has been identified as the greatest trigger for the onset and development of osteoporosis [5], osteoporosis bone treatment must accommodate the reduction of reactive oxygen species (ROS) levels [6]. The ROS chain reaction can cause damage to membrane structures, cell death, and inflammation in tissues [7]. Thus, combining HA with additional ingredients can be aimed at producing bone filler that is biocompatible, bioactive, and has antioxidant activity [8].

Several organic compounds with antioxidant properties have been combined with HA, such as gentamicin [9], catechin [10], quercetin [11], and curcumin [12]. Curcumin (diferuloylmethane) is a linear diarylheptanoid (*E*,*E*)-1,7-bis(4-hydroxy-3-methoxyphenyl)-1,6-heptadiene-3,5-dione) which is the main curcuminoid found in *Curcuma longa* [13]. Commercially, curcumin is usually a mixture of 3 curcuminoids, namely curcumin, demethoxycurcumin, and bisdemethoxycurcumin, with a mass ratio of 77:17:3 [14]. Curcumin has anti-inflammatory, antioxidant, anti-apoptotic, and anti-catabolic effects [15]. However, due to its hydrophobicity and low bioavailability, the therapeutic effect of curcumin as an over-the-counter oral medication is limited [16]. Combining HA with curcumin, besides providing antioxidant activity, also produced antimicrobial and anticancer properties [17-18]. As an anticancer, the HA/curcumin composite can be applied to treat osteosarcoma, the most common type of bone cancer [19-20].

The large number of OH sites on the silica (SiO_2) surface makes SiO_2 a surface-active material. The SiO_2-based bioceramics for biomedical applications have been widely studied [21] due to their ability to support mechanical strength [22-23], increase bioactivity [24], and protect against corrosion [25-27]. *In vitro* and *in vivo* studies showed that SiO_2 has low toxicity and good biocompatibility [28]. Modification of HA with mesoporous SiO_2 produced nanocomposites MCM-48 and HA in which the crystal HA was formed inside the mesoporous SiO_2 structure [29]. The SiO_2 MCM-48/HA composite has the potential to be developed as a controlled drug delivery system [30]. SiO_2-HA nanomaterials can be loaded with a specific agent to promote a targeted delivery of drugs [31], such as polyeugenol [32], silver [33], vitamin D3 [34], sodium fluoride [35], levofloxacin [36], titanium [37], and zirconia [38].

This research studied the effect of the SiO_2 addition on the characteristics of calcium phosphate cement made from HA loaded with curcumin. As a liquid component, a 2.5% Na_2HPO_4 solution was used. HA and SiO_2 will experience co-deposition as the cement sets, and curcumin will be contained in the space between them. The silanol groups of SiO_2 will interact with HA and curcumin so that the properties of the cement will be different from HA/curcumin cement. The HA used in this research was synthesized using the sol-gel method and CTAB as a morphology-directing agent to obtain a homogeneous particle shape and size. The HA/curcumin cement with and without SiO_2 was then immersed in Ringer's solution for 5 d. The chemical and surface morphology studies before and after cement immersion in RS were carried out using FTIR, Raman, XRD, and SEM-EDS instruments. The release behavior of curcumin in RS was conducted using the UV-vis method.

■ EXPERIMENTAL SECTION

Materials

The materials used for HA synthesis were KH_2PO_4 (Merck), $Ca(NO_3)_2{\cdot}4H_2O$ (Merck), NH_4OH (Merck), and CTAB (Sigma Aldrich). The ingredients for making CPC are synthesized HA, curcumin (Merck), and Na_2HPO_4 (Merck). The release test was conducted by using Ringer's solution (Otsu).

Instrumentation

Fourier transform infrared (FTIR, Shimadzu Prestige 21), Fourier transform-Raman (FT-Raman, LabRam Horiba), X-ray diffraction (XRD, PANalytical), scanning electron microscope and energy dispersive X-ray spectroscopy (SEM-EDS, JEOL type JED-2300), ion sputter (Hitachi MC1000), and ultraviolet-visible spectrophotometer (UV-vis Spectrophotometer, Genesys 10S Thermo Scientific) were used in this work.

Procedure

Preparation of hydroxyapatite

About 19.719 g of $Ca(NO_3)_2{\cdot}4H_2O$ and 0.0164 g (0.045 mmol) of CTAB were dissolved in double distilled water to obtain 50 mL of solution I. On the other flask, 50 mL of solution II was made by dissolving 6.804 g KH_2PO_4 and 0.0164 g (0.045 mmol) CTAB with double distilled water. Solution II was added slowly to solution I while stirring with a magnetic stirrer at medium speed. Then, the mixture was added with 15 mL of 32% NH_4OH to obtain a pH > 9. The stirring was continued for 1 h and then left for 24 h at room temperature. The formed precipitate was then washed with 2 L of distilled water and dried in an electric oven at 50 °C for 48 h. The result was then calcined at a temperature of 600 °C for 2 h in an air atmosphere to obtain HA powder.

Preparation of HA/curcumin composite

For the HA/curcumin composite, a certain mass of HA and a certain mass of curcumin (according to Table 1) were placed in a petri dish, and then added with a 2.5% Na_2HPO_4 solution to obtain a certain mass/volume ratio. The mixing process was conducted by using a spatula to produce a homogeneous paste. The paste was then put into a cylindrical mold with a diameter of 1.5 cm and a thickness of 0.5 cm and then allowed to dry at room temperature. The products were then called as HC5–HC25.

Preparation of HA/curcumin/SiO_2 composite

To produce HA/curcumin/SiO_2 composite, a certain mass of HA, curcumin, and SiO_2 were placed in

Table 1. Sample code and composition of hydroxyapatite:curcumin:SiO_2

Sample code	Mass of HA (g)	Mass of curcumin (g)	Mass of SiO_2 (g)	Volume of Na_2HPO_4 2.5% (mL)
HC5	0.95	0.50	-	1.00
HC10	0.90	0.10	-	1.00
HC15	0.85	0.15	-	1.00
HC20	0.80	0.20	-	1.00
HC25	0.75	0.25	-	1.00
HCS4	0.75	0.25	0.25	1.40
HCS5	0.75	0.25	0.20	1.30
HCS6	0.75	0.25	0.17	1.30
HCS7	0.75	0.25	0.14	1.20
HCS8	0.75	0.25	0.13	1.20

Table 2. Sample code for the release test

Sample code	Time of immersion (d)
HC25_1	1
HC25_2	2
HC25_3	3
HC25_4	4
HC25_5	5
HCS4_1	1
HCS4_2	2
HCS4_3	3
HCS4_4	4
HCS4_5	5

a petri dish, and then added with a 2.5% Na_2HPO_4 solution to obtain a certain mass/volume ratio. The same treatment as in the production of HA/curcumin was then applied. The products were then called HCS0–HCS8.

Release test

The release test was conducted by using HC25 and HCS4 samples. The samples were placed in a chamber that contained 50 mL of Ringer's solution for 1–5 d. The released curcumin was tested by UV-vis spectrophotometer. The sample code can be seen in Table 2.

Characterizations

The resulting semen was analyzed by FTIR: measurements were carried out using the KBr pellet method at wave numbers 4000–350 cm^{-1}, and FT-Raman spectrum was recorded using an Nd:YAG laser with an excitation wavelength of 1064 nm. Each spectrum is the average of two repeated measurements of 200 scans each and a resolution of 2 cm^{-1}. The laser power of the source was maintained at 100 mW throughout the measurements and a liquid nitrogen-cooled Ge detector was used. Crystal analysis was conducted by using XRD at start position $2\theta = 5.0054°$, end position $2\theta = 89.9884°$, step size $2\theta = 0.0170°$ and scan step time = 10.1600 s. Surface morphology was identified by SEM-EDS: JEOL and ion sputter was used to coat the samples with gold at a thickness of 1 nm.

■ RESULTS AND DISCUSSION

The appearance of HA/curcumin composites (HC5–HC25) and HA/curcumin/SiO_2 (HCS0–HCS8) are shown in Fig. 1. These composites were produced by using 2.5% Na_2HPO_4 as a solvent (liquid component). Table 1 shows that the liquid/powder ratio of HA/curcumin composites are same, in which the change in HA and curcumin composition did not change the amount of solvent needed. The liquid/powder ratio increases to 1.2–1.4 by the addition of 0.13–0.25 g SiO_2. For HC5–HC25 samples the color intensity of the composite increases with the increase in curcumin percentage (Fig. 1(a)). At the same percentage of curcumin (25%), the color intensity decreases with increased SiO_2 content (Fig. 1(b)). This indicated that the presence of SiO_2 decreased the amount of curcumin on the composite surface.

The results of FTIR analysis for HC5–HC25 and HCS0–HCS8 samples can be seen in Fig. 2. The composites produced from varying 5–25% curcumin

Fig 1. The appearance of (a) HC5–HC25 and (b) HC25–HCS8 samples

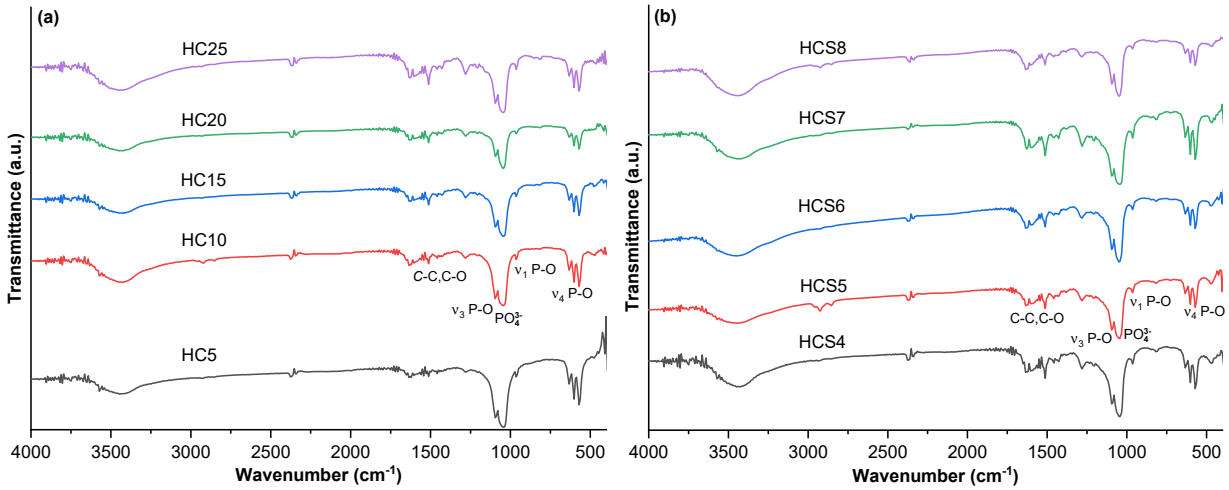

Fig 2. FTIR spectra of (a) HC5–HC25 and (b) HCS4–HCS8 sample

concentrations (HC5–HC25) (Fig. 2(a)) show the same spectra pattern. The peak around 3440 cm^{-1} indicates the O–H stretching mode of HA and curcumin. A small peak at 3574 cm^{-1} indicates the symmetric stretching of H_2O. The presence of adsorbed water was proofed by the appearance of bending H_2O at 1627 cm^{-1} [17]. The specific vibrational energy belonging to the phosphate group of HA appears as a sharp peak at 1095 and 1049 cm^{-1}, which is ν_3 asymmetric bending P–O. The peak at 964 cm^{-1} indicates the presence of ν_1 stretching P–O. Bending vibrations (ν_4) O–P–O appear at 601 and 570 cm^{-1} [39-40]. The characteristic peaks of curcumin appear at 1505 cm^{-1} due to the mixed C–C and C–O vibrations, 1634 cm^{-1} due to the stretching vibration of the benzene ring skeleton, 1430 cm^{-1} due to aliphatic C–H in-plane bending vibrations, and 1160 cm^{-1} due to the enol peak for C–O–C [41-42]. Those peak's intensity increases with the increase of curcumin percentage. Due to the clearest spectra pattern shown by the composite with 25% curcumin, henceforth HC25 was used to study the effect of SiO_2 content. Spectra of HCS4–HCS8 (Fig. 2(b)) have the same spectra pattern as HC25, only the presence of the Si–O–Si group, which should be confirmed by the appearance of a peak at 1088 cm^{-1} turns out to overlap with the peak asymmetric stretching vibration of PO_4^{3-} [43]. Then, to study the effect of SiO_2 addition on the composite properties, the HCS4 sample was used due to the highest content of SiO_2. HC25 and HCS4 samples were then immersed in Ringer's solution (RS) for 5 d. RS contains NaCl (8.6 g/L), KCl (0.3 g/L), and $CaCl_2{\cdot}2H_2O$ (0.33 g/L), which is close to the estimated physiological concentrations in the extracellular space. The FTIR spectra of HC25 and HCS4, before and after immersion in RS, can be seen in Fig. 3. The spectra pattern of HC25

after being immersed in RS for 1–5 d looked the same, except for 4 d of immersion, in which the peaks appear most sharp than the others (Fig. 3(a)). These phenomena also happened to HCS4 (Fig. 3(b)). As expected, water and ions in RS did not produce new compounds because new compounds will affect the biocompatibility properties of the composites [12,44].

Functional group analysis using Raman for the HC25 sample before and after immersion in RS for 5 d can be seen in Fig. (4a). The spectra of HC25 indicated the presence of HA due to the appearance of P–O vibrations at 960.90 cm^{-1} [45]. The presence of curcumin in the form of enol (demethoxycurcumin) was proven by the absence of a peak for ν(C=O) around 1650–1800 cm^{-1} [14,46]. The peak related to the presence of ν(C=C) and ν(C=O) in the curcumin structure appears at 1625.84 cm^{-1} and the peak at 1599.60 cm^{-1} indicates the vibration of ν(C–C_{ring}) from the aromatic ring. The Raman spectrum after immersion shows that the P–O vibration of HA appears at 960.82 cm^{-1}. Curcumin in the enol form is proven by the presence of ν(C=C) and ν(C=O) peaks at 1625.84 cm^{-1}, and the peak at 1600.01 cm^{-1} indicates the ν(C–C_{ring}) vibration of the aromatic ring. Other peaks that specifically belong to curcumin appear at 570.18, 1150.28, 1182.11, 1249.23, and 1429.74 cm^{-1} [17,47]. The sharp peak of curcumin indicates that immersion in RS for up to 5 d causes curcumin to be exposed on the surface. This is very beneficial in its application because antioxidant and antibacterial activity occurs at the interface. Thus, curcumin activity increases due to the interaction of HC25 with water and ions in RS. It can also be seen from the brighter intensity of the yellow color in

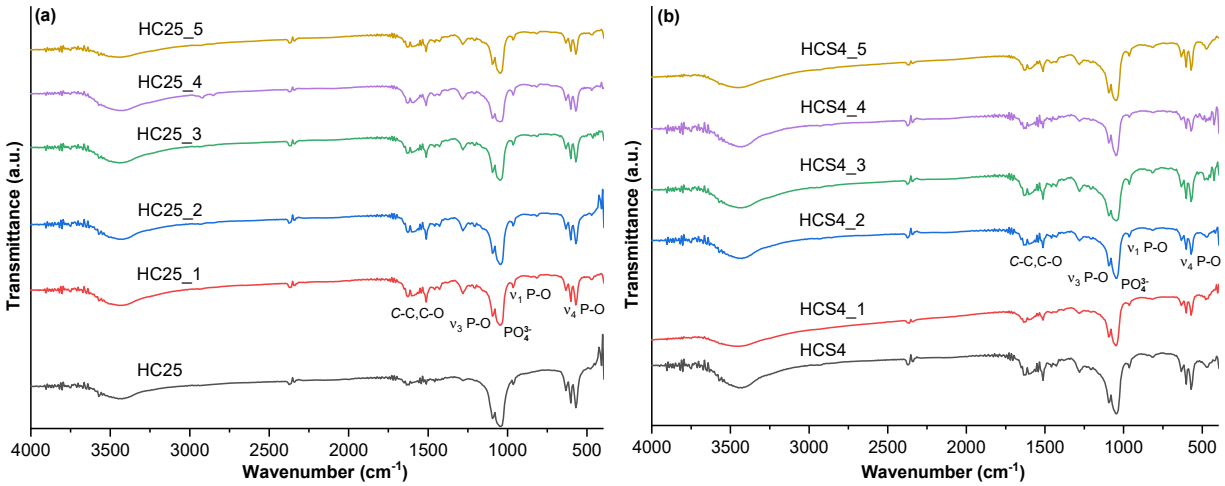

Fig 3. FTIR spectra of (a) HC25 and (b) HCS4 before and after immersion in Ringer's solution for 1–5 d

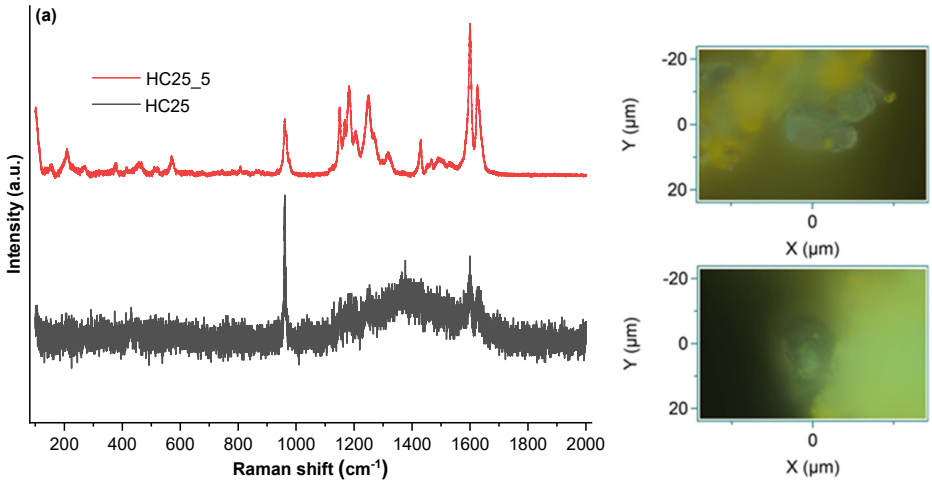

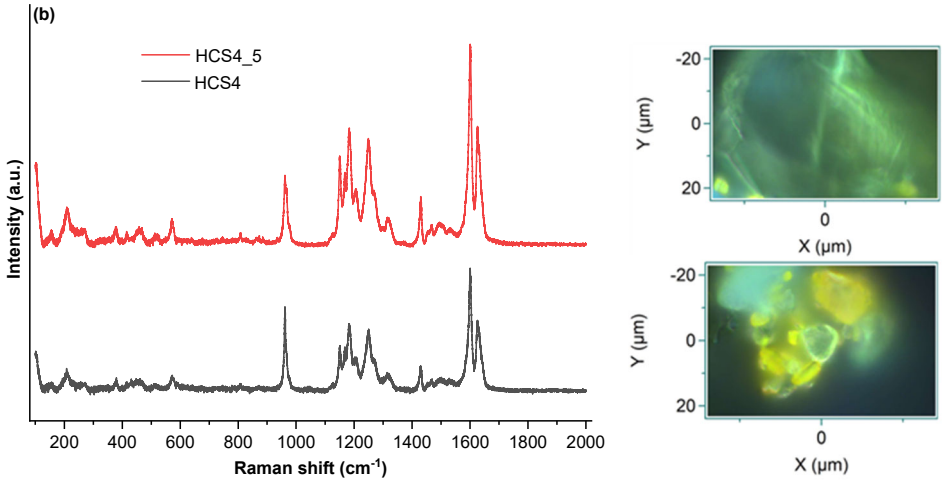

Fig 4. Raman spectra of (a) HC25 and (b) HCS4, before and after immersion in Ringer's solution for 5 d

the scanning position image after HC25 was immersed in RS for 5 d.

Raman spectra for HCS4 and HCS4_5 are shown in Fig. 4(b). Both spectra show the same pattern with sharp peaks. The presence of HA in HCS4 is indicated by the P–O vibration at 961.33 cm^{-1}, while in HCS4_5 it is 961.19 cm^{-1}. The enol form of curcumin is proven by the presence of ν(C=C) and ν(C=O) peaks at 1625.29 cm^{-1}, the peak at 1600.96 cm^{-1} indicates the ν(C–C_{ring}) vibration of the aromatic ring. Other peaks that specifically belong to curcumin appear at 570.00, 1151.35, 1183.25, 1250.27, and 1428.31 cm^{-1}. The sharp peak of curcumin indicates curcumin is on the surface. In scanning with an area of 40 × 60 μm, SiO_2 particles were not detected, so no specific peaks appeared from the Si–O–Si vibration. After immersing HCS4 in RS for up to 5 d (HCS4_5), it turned out that the peaks belonging to curcumin appeared with a higher intensity than the HCS4 spectrum. The phenomena happened to HC25, where immersion in RS causes the curcumin to be increasingly exposed on the surface. The image at the scanning position shows that the distribution of the yellow color of curcumin is most even on the surface of HCS4_5, which indicates that SiO_2 plays a role in increasing the distribution of curcumin in the composite.

The change in crystal properties due to the immersion of HC25 for 5 d (HCS25_5) was studied by XRD analysis (Fig. 5). For HC25, the XRD pattern shows that the composite contains HA according to JCPDS-09-0432 due to the appearance of sharp peaks at 2θ = 25.94°, 31.84°, 32.27°, 32.98°, and 34.13° were indexed to the (002), (211), (112), (300), and (202) diffraction planes of the hexagonal structure [48]. Specific peaks of curcumin appear as a sharp peak at 2θ = 17.44° [49]. The ratio of

Table 3. Peaks properties of XRD diffractogram for HC25 and HC25_5

hkl	2θ (°)		d-spacing (Å)		FWHM (°2θ)	
	HC25	HC25_5	HC25	HC25_5	HC25	HC25_5
100	10.91	-	8.1002	-	0.5035	-
110	17.44	17.45	5.0817	5.0785	0.1859	0.1713
111	23.50	23.52	3.7823	3.7800	0.1956	0.1726
002	25.95	25.94	3.4309	3.4313	0.4930	0.4268
212	29.01	29.00	3.0759	3.0762	0.4909	0.4288
211	31.85	31.84	2.8077	2.8080	0.4891	0.4310
112	32.27	32.26	2.7722	2.7725	0.4888	0.4314
300	32.98	32.98	2.7136	2.7139	0.4883	0.4320
202	34.13	34.13	2.6246	2.6249	0.4876	0.4331

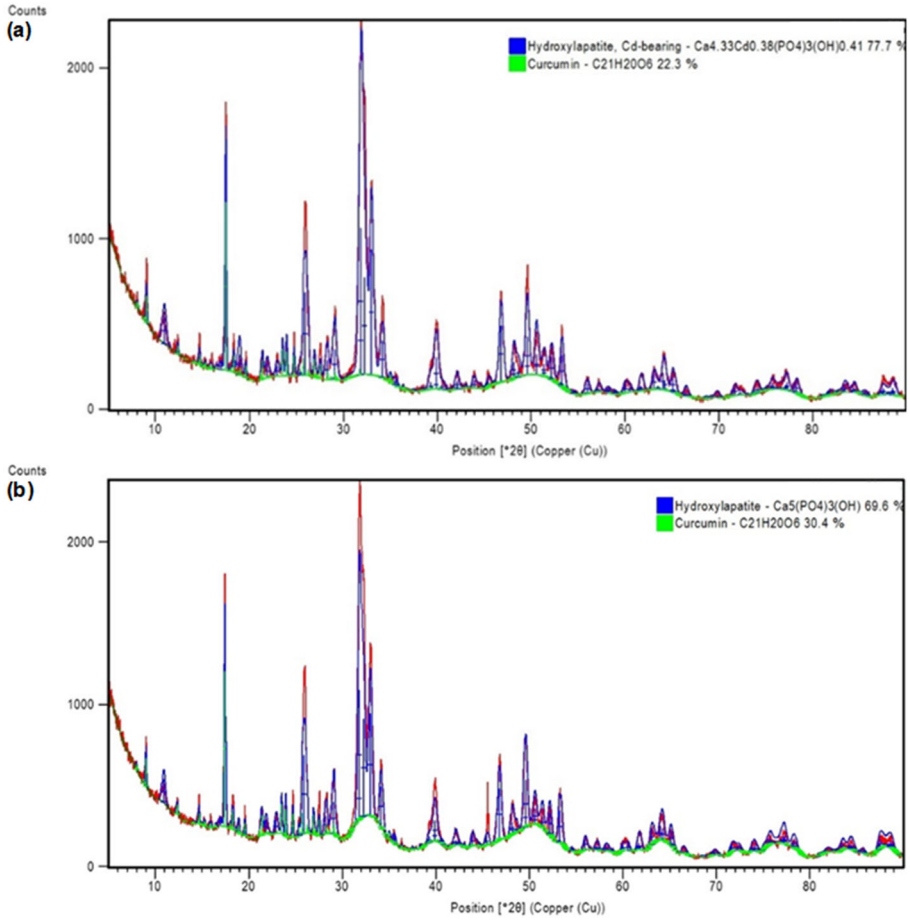

Fig 5. The refinement result of XRD data for (a) HC25 and (b) HC25_5

HA:curcumin is 77.7%:22.3%, then changed to 69.6%:30.4% after HSC25 was immersed in RS for 5 d. These data are related to the Raman data in which curcumin is exposed to the surface more after the immersion process. The 2θ is slightly shifted to the left side, or the d-spacing slightly increases (Table 3). The FWHM decreased significantly, indicating that the crystallite size increased due to the crystal plane arrangement. According to Scherrer's formula, a smaller FWHM value produced a larger crystallite size.

The diffraction patterns of both HCS4 and HCS4_5 samples (Fig. 6) looked the same as those of HC25. The ratio of HA:curcumin for HCS4 = 77.5%:22.5% change into 70.1%:29.9% for HCS4_5. These data are consistent with the phenomena for the HC25 sample. However, 2θ is shifted to the right and the d-spacing is decreased due to the immersion in RS. As in the HC25 sample, the FWHM decreases significantly, or the crystal area increases (Table 4).

The results of imaging with SEM for the HC25 sample up to 25,000 times magnification are shown in Fig. 7(a). It can be seen that the spherical and nano-sized particles agglomerate into particles with a length of up to 5 μm. This agglomeration occurs due to strong intermolecular interactions between Ca^{2+}, PO_4^{3-}, and OH^- ions in each HA molecule. This is consistent with previous research, which states that HA has a zeta potential of −43,895 ± 0.061, which means HA tends to agglomerate in water [43]. The interaction of the HC25 surface with ions in the RS causes crystal growth (Fig. 7(b)). This is proven by the larger particle size in the HC25_5 sample which is the same shape as that of HC25. The tendency of the HA surface to attract ions is caused by the negative charge that the HA surface has.

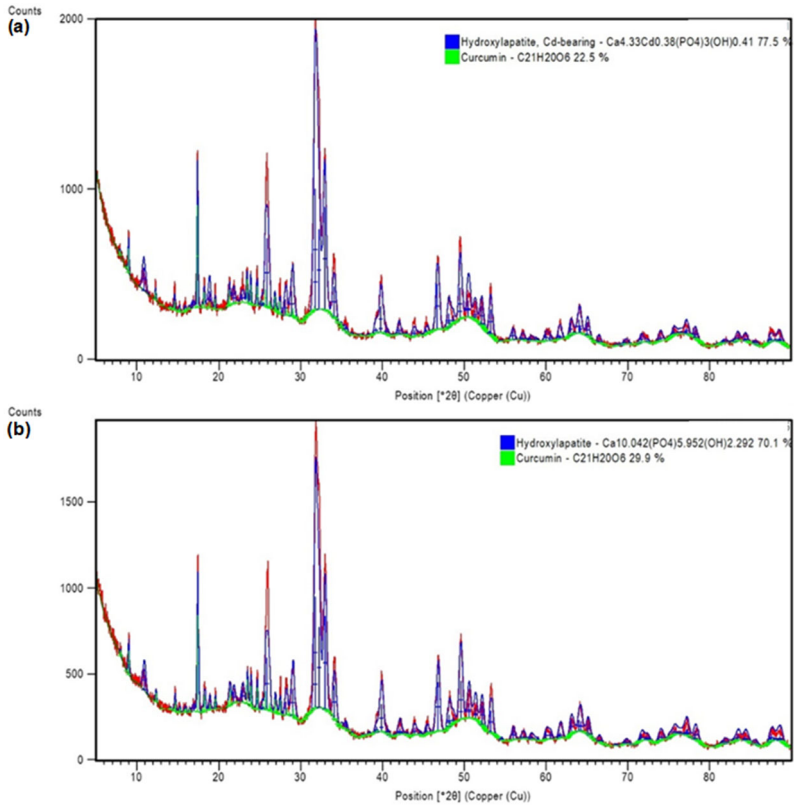

Fig 6. The refinement result of XRD data for (a) HCS4 and (b) HCS4_5

Table 4. Peaks properties of XRD diffractogram for HCS4 and HCS4_5 based on JCPDS card no 090432

hkl	2θ (°)		d-spacing (Å)		FWHM left (°2θ)	
	HCS4	HCS4_5	HCS4	HCS4_5	HCS4	HCS4_5
100	10.8700	10.9100	8.1306	8.1018	0.4878	0.4521
110	17.4000	17.4500	5.0922	5.0785	0.1733	0.1897
111	23.4700	23.5200	3.7872	3.7799	0.1809	0.1940
201	-	25.7100	-	3.4615	-	0.1961
002	25.9000	25.9500	3.4366	3.4308	0.4803	0.4552
210	28.9600	29.0000	3.0803	3.0762	0.4789	0.4569
211	31.8000	31.8400	2.8114	2.8079	0.4777	0.4588
112	32.2200	32.2600	2.7759	2.7722	0.4775	0.4591
300	32.9400	32.9800	2.7171	2.7139	0.4772	0.4596
202	34.0900	34.1300	2.6279	2.6246	0.4767	0.4605

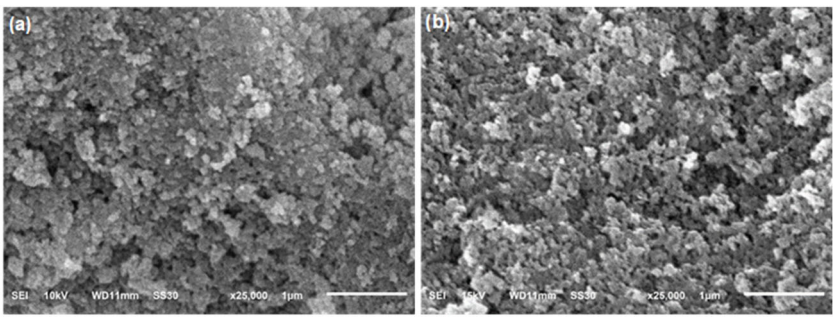

Fig 7. SEM image of (a) HC25 and (b) HC25_5

This causes positively charged ions such as Na^+, K^+, and Ca^{2+} in RS to be attracted to the HA surface, resulting in crystal growth. Agglomeration of HC25_5 particles produced agglomerates 2 times bigger than the agglomerates of HC25.

The presence of SiO_2 in the HCS4 produced a composite morphology profile that was the same as HC25 (Fig. 8(a)). The SiO_2 particle's shape in HCS4 is rod-like with sharp edges and a length of up to 70 μm or larger than HA particles. Meanwhile, HA particles are spherical and nano-sized and agglomerate to produce irregular agglomerates. Soaking HCS4 in RS for 5 d caused the SiO_2 particle size to degrade into smaller particles, might be due to some of the SiO_2 being dissolved (Fig. 8(b)). Then, dissolved SiO_2 was deposited on the HA surface, resulting in a denser surface. HA and SiO_2 form a composite on the HA surface. It can be estimated that HCS4 has greater mechanical strength due to a longer immersion time in RS.

The EDS test results of HC25 are shown in Fig. 9(a). From the 2 scanning positions, the same profile is obtained for the dispersed X-ray energy, indicating that the cement has a uniform surface. The results of elements mapping on the surface of HC25 produce the following average atomic levels: Ca (21.12%), P (10.97%), O (52.44%), and C (15.48%) (Table 5). The elements Ca, P, and O represent the HA molecule, while curcumin is represented by the elements C and O. The Ca/P ratio on the surface of HC25 is 1.92 or greater than the Ca/P HA molar ratio (1.67). This indicates that more Ca elements are found on the surface. The O element found abundantly on the surface, is expected to increase the biocompatibility of cement. The high percentage of element C indicates that curcumin is also found in abundance on surfaces. Considering that antioxidant activity is a phenomenon that occurs at the interface, the presence of curcumin on the cement surface is highly expected. Analysis with EDS on the HC25_5 surface also produces the same dispersed X-ray energy profile at 2 scanning positions (Fig. 9(b)). There was a change in the percentage of elements on the surface of HC25 after immersion in RS for 5 d. The Ca element decreased to 18.05%, P decreased to 9.47% while the amount of O increased to 57.25%. The Ca/P ratio on the surface is still relatively the same at 1.91. Otherwise, the element C content decreases to 15.24%. It can happen due to the low solubility of curcumin in water. Curcumin can be

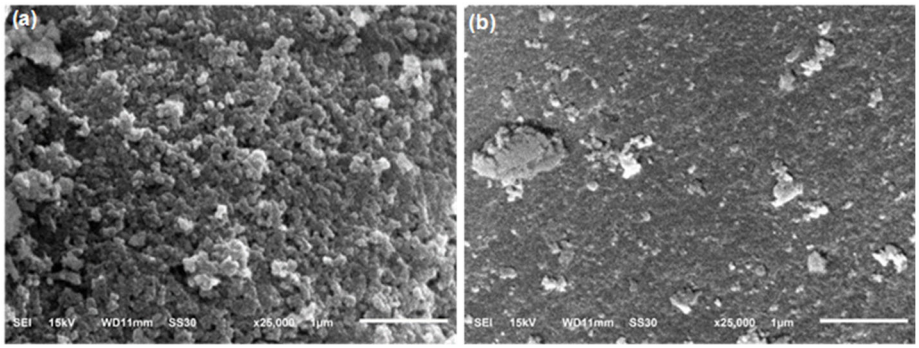

Fig 8. SEM image of (a) HCS4 and (b) HCS4_5

Table 5. Elements composition on HC25 and HC25_5 surface

Element	Atom (%)					
	HC25			HC25_5		
	1	2	mean	1	2	mean
Ca	22.14	20.09	21.12	17.96	18.14	18.05
P	11.29	10.65	10.97	9.39	9.54	9.47
O	51.43	53.45	52.44	56.78	57.72	57.25
C	15.15	15.81	15.48	15.87	14.60	15.24
Ca/P			1.92			1.91

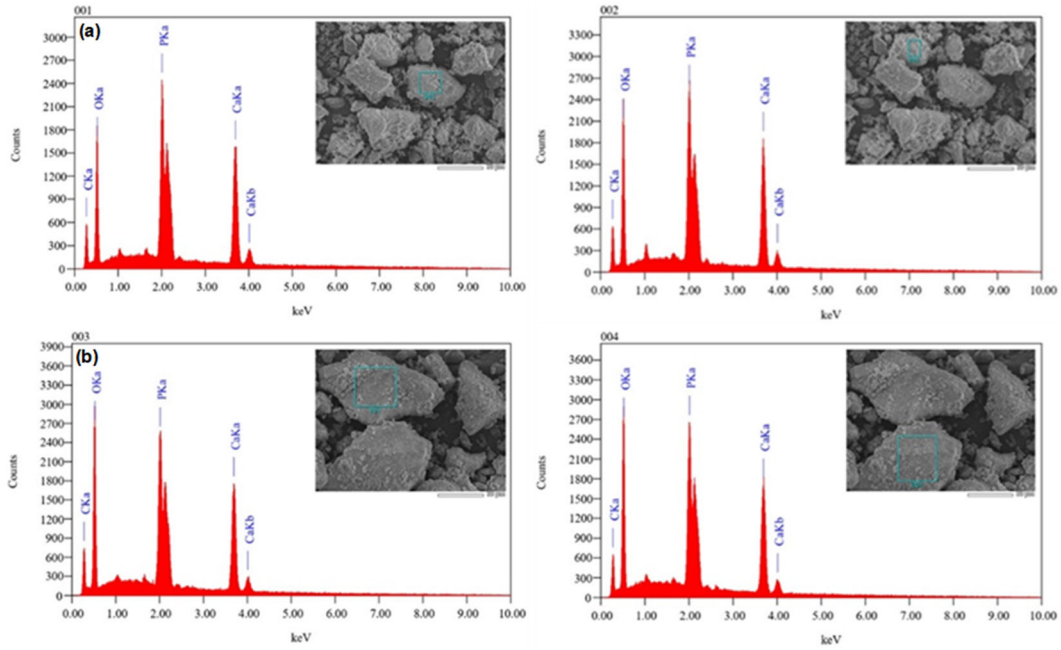

Fig 9. EDS data for (a) HC25 and (b) HC25_5

maintained on the cement surface ensuring that its respective antioxidant activity can last for a long period. The Ca/P ratio, which is the same as HC25 indicates that the deposit of ions on the cement surface still maintains the structure of HA on the surface. Increasing the amount of element O is expected to correlate with increasing biocompatibility of HC25.

The elements mapping of HC25 and HC25_5 can be seen in Fig. 10. On the same scale, the particle size on the surface of HC25_25 is larger than the HC25 particles, or crystal growth occurs due to the interaction of the HC25 surface with ions in RS. The presence of ions with a 2+ charge becomes a bridge for small particles to form agglomerates. The elements Ca, P, and O appear to have high intensity, meaning all three are often found on the surface. This is different from element C which appears between HA particles. The curcumin in the HC25 composite is in the deeper part. The abundance of the cement surface with HA ensures a bond between the cement and bone tissue when the cement is used as a bone filler so that new tissue is formed between the cement and bone. The compatibility of HA in HC25 cement can

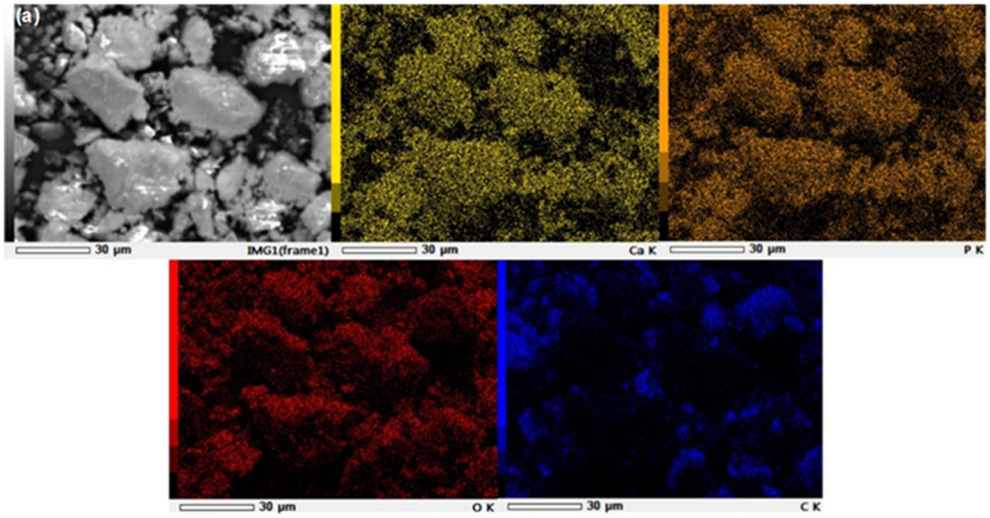

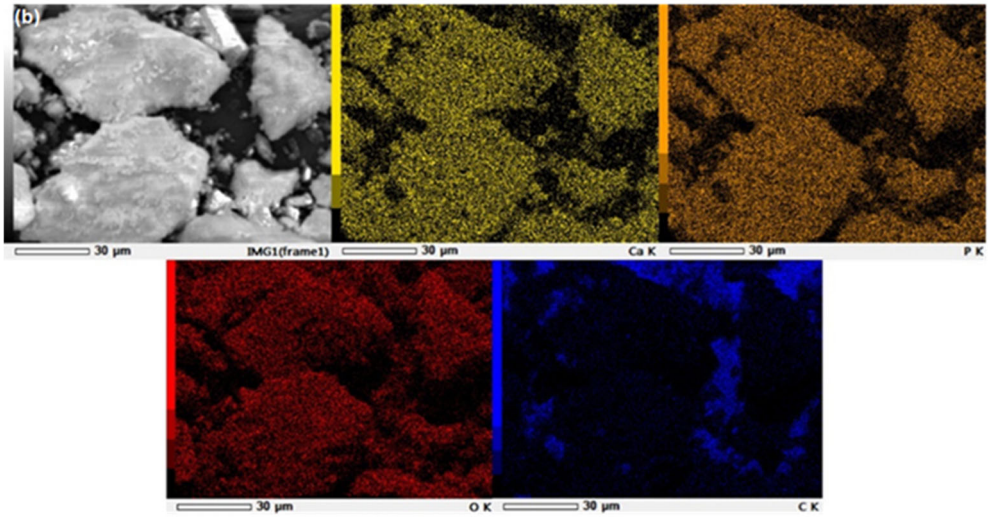

Fig 10. Elements mapping on the surface of (a) HC25 and (b) HC25_5

be maintained. From the mapping results, the surface of HC25 is not flat or porous. This type of surface is very good for biomaterials because it supports the attachment of bone cells, proteins, and ions from body fluids. In this way, the cement deformation process can take place, and new bone tissue can form.

EDS data for samples HCS4 and HCS4_5 is shown in Fig. 11. Scanning at 2 positions shows different peak patterns, indicating that the surfaces observed contain 2 different particles. One is SiO_2 and the other is HA, while curcumin is distributed between the 2 particles. The HCS4 sample, which initially had a Ca/P ratio = 1.98 changed to 2.18 after soaking for 5 d in RS (Table 6). Soaking HCS4 in RS only slightly released curcumin due to the low solubility of curcumin in water. All elements tend to decrease in quantity except O, which increases significantly. The elemental mapping results (Fig. 12) show that the size of the SiO_2 particles decreases after immersion in the RS. On the other hand, the HA particle size becomes larger, as in the HC25 sample. HA is also

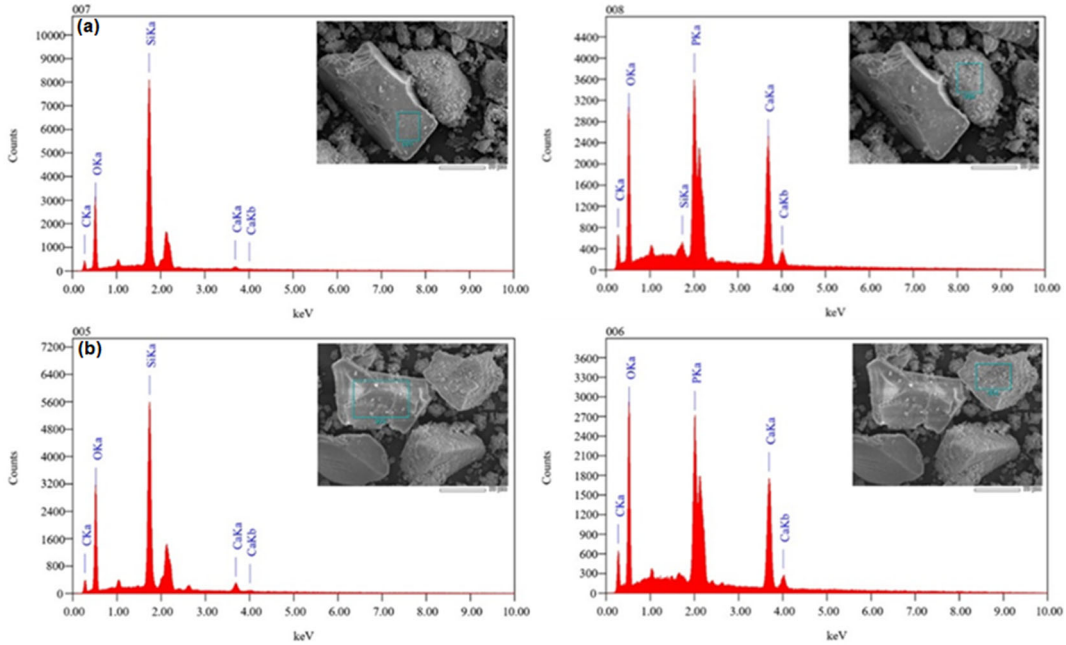

Fig 11. EDS data for (a) HCS4 and (b) HCS4_5

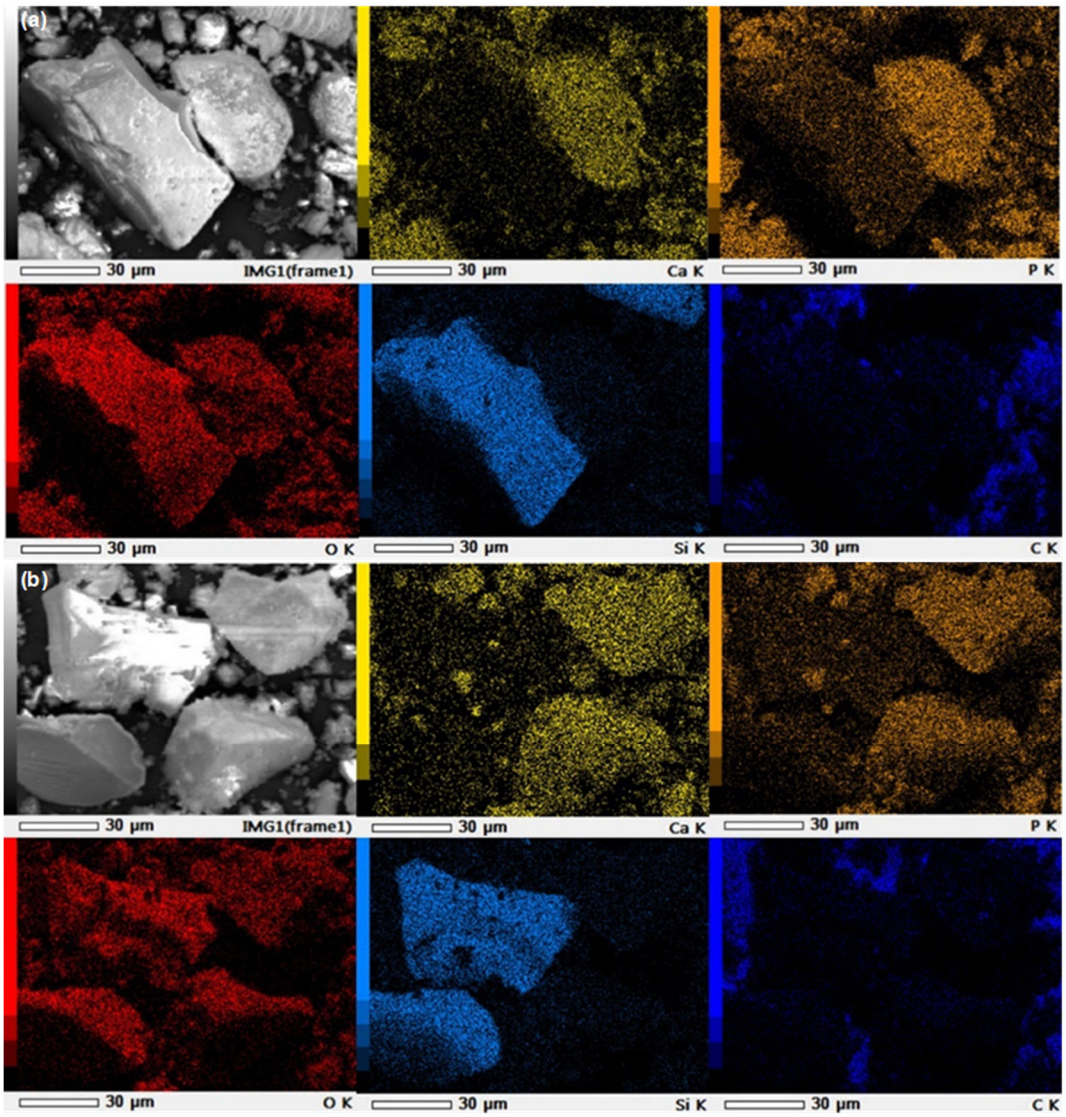

Fig 12. Elements mapping on the surface of (a) HCS4 and (b) HCS4_5

Table 6. Elements composition on HCS4 and HCS4_5 surface

Element	Atom (%)					
	HCS4			HCS4_5		
	1	2	Mean	1	2	Mean
Ca	1.23	20.93	11.08	3.03	18.08	10.56
P	0.00	11.20	5.60	0.00	9.69	4.85
O	43.85	54.81	49.33	51.60	58.22	54.91
Si	33.45	0.47	16.96	26.40	0.00	13.20
C	21.48	12.59	17.04	18.97	14.01	16.49
Ca/P			1.98			2.18

formed on the SiO_2 surface, which indicates that SiO_2 has osteoinductive properties. As in HC25, curcumin is filling the space between HA and SiO_2.

Analysis using UV-vis for the RS after soaking for 1–5 d showed different release behavior of curcumin in samples HC25 and HCS4 (Fig. 13). The presence of

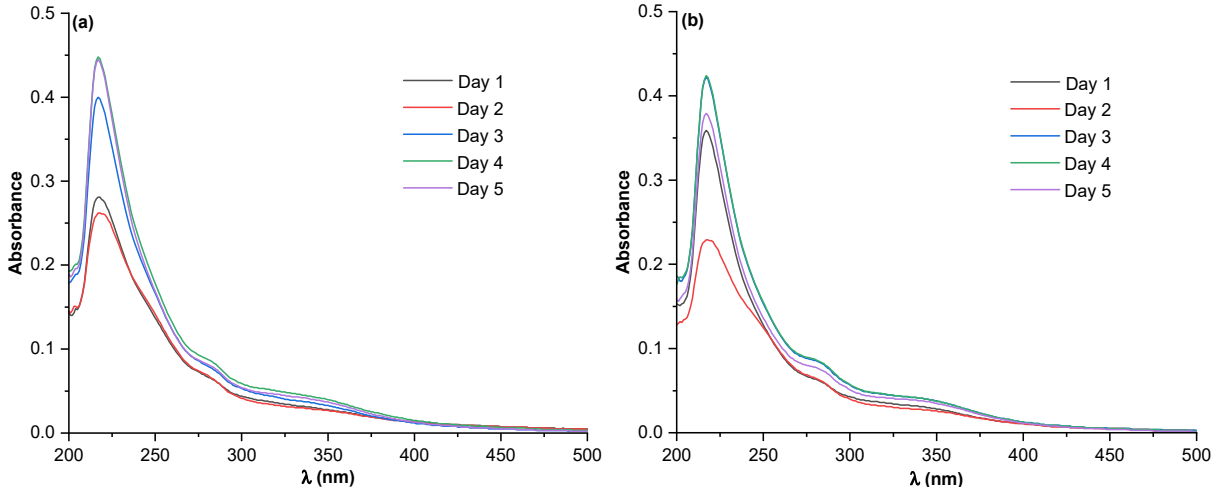

Fig 13. Release test of curcumin in RS for (a) HC25 and (b) HCS4

curcumin was identified by the light adsorption at 200–500 nm [50]. For HC25, the release of curcumin tended to increase with time of soaking in RS. Otherwise, for the HCS4 sample, the release of curcumin fluctuated or became non-linear with soaking time. These results are consistent with the previous study, in which compositing curcumin prolongs the release of curcumin [45,49]. Thus, the presence of SiO_2 inhibits the release of curcumin into RS.

■ CONCLUSION

The addition of 25% SiO_2 to the HA/curcumin composite significantly impacted the interaction between HA-curcumin and HA/curcumin-RS. The behavior of the composite in the RS also changes, which is characterized by the formation of particles with a larger size and a larger Ca/P ratio due to the interaction of the ions in the RS with the composite surface. The release of curcumin from the composite is also inhibited due to the presence of SiO_2. Curcumin tends to remain on the surface of the composite, so it can be predicted that its antioxidant and antibacterial activity can be maintained as long as the HA/curcumin/SiO_2 composite is used as a bone filler.

■ ACKNOWLEDGMENTS

The authors gratefully acknowledge the Faculty of Mathematics and Sciences, Universitas Diponegoro, Semarang, Indonesia for the financial support through the research grant "Riset Madya" with contract number: 1263J/UN7.5.8/PP/2022.

■ CONFLICT OF INTEREST

All the authors have no conflict of interest.

■ AUTHOR CONTRIBUTIONS

All authors carried out the experiment, analyzed data, wrote, revised the manuscript, and agreed to the final version of this manuscript.

■ REFERENCES

[1] Langdahl, B., 2020, Treatment of postmenopausal osteoporosis with bone-forming and antiresorptive treatments: Combined and sequential approaches, *Bone*, 139, 115516.

[2] Deng, Y., Wei, W., and Tang, P., 2022, Applications of calcium-based nanomaterials in osteoporosis treatment, *ACS Biomater. Sci. Eng.*, 8 (2), 424–443.

[3] Wu, T., Sun, J., Tan, L., Yan, Q., Li, L., Chen, L., Liu, X., and Bin, S., 2020, Enhanced osteogenesis and therapy of osteoporosis using simvastatin loaded hybrid system, *Bioact. Mater.*, 5 (2), 348–357.

[4] Zhao, Y., Li, Z., Jiang, Y., Liu, H., Feng, Y., Wang, Z., Liu, H., Wang, J., Yang, B., and Lin, Q., 2020, Bioinspired mineral hydrogels as nanocomposite scaffolds for the promotion of osteogenic marker expression and the induction of bone regeneration in osteoporosis, *Acta Biomater.*, 113, 614–626.

[5] Rasool, N., Negi, D., and Singh, Y., 2023, Thiol-functionalized, antioxidant, and osteogenic

mesoporous silica nanoparticles for osteoporosis, *ACS Biomater. Sci. Eng.*, 9 (6), 3535–3545.

[6] Abdollahi, M., Larijani, L., Rahimi, R., and Salari, O., 2005, Role of oxidative stress in osteoporosis, *Therapy*, 2 (5), 787–796.

[7] Markovic, Z., and Trajkovic, V., 2008, Biomedical potential of the reactive oxygen species generation and quenching by fullerenes (C_{60}), *Biomaterials*, 29 (26), 3561–3573.

[8] Pandey, A., Midha, S., Sharma, R.K., Maurya, R., Nigam, V.K., Ghosh, S., and Balani, K., 2018, Antioxidant and antibacterial hydroxyapatite-based biocomposite for orthopedic applications, *Mater. Sci. Eng., C*, 88, 13–24.

[9] Stevanović, M., Đošić, M., Janković, A., Kojić, V., Vukašinović-Sekulić, M., Stojanović, J., Odović, J., Crevar Sakač, M., Rhee, K.Y., and Mišković-Stanković, V., 2018, Gentamicin-loaded bioactive hydroxyapatite/chitosan composite coating electrodeposited on titanium, *ACS Biomater. Sci. Eng.*, 4 (12), 3994–4007.

[10] Sistanipour, E., Meshkini, A., and Oveisi, H., 2018, Catechin-conjugated mesoporous hydroxyapatite nanoparticle: A novel nano-antioxidant with enhanced osteogenic property, *Colloids Surf., B*, 169, 329–339.

[11] Forte, L., Torricelli, P., Boanini, E., Gazzano, M., Rubini, K., Fini, M., and Bigi, A., 2016, Antioxidant and bone repair properties of quercetin-functionalized hydroxyapatite: An *in vitro* osteoblast-osteoclast-endothelial cell co-culture study, *Acta Biomater.*, 32, 298–308.

[12] Eren, T., Baysal, G., and Doğan, F., 2020, Biocidal activity of bone cements containing curcumin and pegylated quaternary polyethylenimine, *J. Polym. Environ.*, 28 (9), 2469–2480.

[13] Marino, V., Battaglini, M., Moles, N., and Ciofani, G., 2022, Natural antioxidant compounds as potential pharmaceutical tools against neurodegenerative diseases, *ACS Omega*, 7 (30), 25974–25990.

[14] Perera, K.D.C., Weragoda, G.K., Haputhanthri, R., and Rodrigo, S.K., 2021, Study of concentration dependent curcumin interaction with serum biomolecules using ATR-FTIR spectroscopy combined with Principal Component Analysis (PCA) and Partial Least Square Regression (PLS-R), *Vib. Spectrosc.*, 116, 103288.

[15] Pérez-Lozano, M.L., Cesaro, A., Mazor, M., Esteve, E., Berteina-Raboin, S., Best, T.M., Lespessailles, E., and Toumi, H., 2021, Emerging natural-product-based treatments for the management of osteoarthritis, *Antioxidants*, 10 (2), 265.

[16] Cheng, D., Li, W., Wang, L., Lin, T., Poiani, G., Wassef, A., Hudlikar, R., Ondar, P., Brunetti, L., and Kong, A.N., 2019, Pharmacokinetics, pharmacodynamics, and PKPD modeling of curcumin in regulating antioxidant and epigenetic gene expression in healthy human volunteers, *Mol. Pharmaceutics*, 16 (5), 1881–1889.

[17] Sebastiammal, S., Lesly Fathima, A.S., Devanesan, S., AlSalhi, M.S., Henry, J., Govindarajan, M., and Vaseeharan, B., 2020, Curcumin-encased hydroxyapatite nanoparticles as novel biomaterials for antimicrobial, antioxidant and anticancer applications: A perspective of nano-based drug delivery, *J. Drug Delivery Sci. Technol.*, 57, 101752.

[18] Hani, U., Jaswanth Gowda, B.H., Siddiqua, A., Wahab, S., Begum, M.Y., Sathishbabu, P., Usmani, S., and Ahmad, P.M., 2023, Herbal approach for treatment of cancer using curcumin as an anticancer agent: A review on novel drug delivery systems, *J. Mol. Liq.*, 390, 123037.

[19] Marinho, J.P.N., Neme, N.P., Matos, M.J.S., Batista, R.J.C., Macedo, W.A.A. Gastelois, P.L., Gomes, D.A., Rodrigues, M.A., Cipreste, M.F., and Sousa, E.M.B., 2023, Nanostructured system based on hydroxyapatite and curcumin: A promising candidate for osteosarcoma therapy, *Ceram. Int.*, 49 (12), 19932–19949.

[20] Dhatchayani, S., Vijayakumar, S., Sarala, N., Vaseeharan, B., and Sankaranarayanan, K., 2020, Effect of curcumin sorbed selenite substituted hydroxyapatite on osteosarcoma cells: An *in vitro* study, *J. Drug Delivery Sci. Technol.*, 60, 101963.

[21] Ferrairo, B.M., Mosquim, V., de Azevedo-Silva, L.J., Pires, L.A., Padovini, D.S.S., Magdalena, A.G., Fortulan, C.A., Lisboa-Filho, P.N., Rubo, J.H., and

Borges, A.F.S., 2023, Experimental silica-based bioceramic composite added with nano-sized bovine hydroxyapatite: Synthesis and characterization, *Silicon*, 15 (16), 7171–7181.

[22] Liu, F., Jiang, X., Zhang, Q., and Zhu, M., 2014, Strong and bioactive dental resin composite containing poly(bis-GMA) grafted hydroxyapatite whiskers and silica nanoparticles, *Compos. Sci. Technol.*, 101, 86–93.

[23] Shahgholi, M., Firouzi, P., Malekahmadi, O., Vakili, S., Karimipour, A., Ghashang, M., Hussain, W., Kareem, H.A., and Baghaei, S., 2022, Fabrication and characterization of nanocrystalline hydroxyapatite reinforced with silica-magnetite nanoparticles with proper thermal conductivity, *Mater. Chem. Phys.*, 289, 126439.

[24] Yuan, X., Xu, Y., Lu, T., He, F., Zhang, L., He, Q., and Ye, J., 2022, Enhancing the bioactivity of hydroxyapatite bioceramic via encapsulating with silica-based bioactive glass sol, *J. Mech. Behav. Biomed. Mater.*, 128, 105104.

[25] Sidane, D., Khireddine, H., Bir, F., Yala, S., Montagne, A., and Chicot, D., 2017, Hydroxyapatite-TiO_2-SiO_2-coated 316L stainless steel for biomedical application, *Metall. Mater. Trans. A*, 48 (7), 3570–3582.

[26] Evcin, A., and Bohur, B.G., 2019, Coating of different silica sources containing hydroxyapatite for Ti_6Al_4V metal substrate using HVOF technique, *Arabian J. Geosci.*, 12 (6), 220.

[27] Mahalingam, V., Sivaraju, M., and Shanmugasundaram, P., 2023, Synthesis of silica/hydroxyapatite nanocomposites using rice husk and fish scale for corrosion protection application, *Silicon*, 15 (13), 5603–5613.

[28] Albert, K., Huang, X.C., and Hsu, H.Y., 2017, Bio-templated silica composites for next-generation biomedical applications, *Adv. Colloid Interface Sci.*, 249, 272–289.

[29] Lenji, R.K., Nourbakhsh, A.A., Nourbakhsh, N., Nourbakhsh, M., and Mackenzie, K.J.D., 2017, Phase formation, microstructure and setting time of MCM-48 mesoporous silica nanocomposites with hydroxyapatite for dental applications: Effect of the Ca/P ratio, *Ceram. Int.*, 43 (15), 12857–12862.

[30] Pajchel, L., and Kolodziejski, W., 2018, Synthesis and characterization of MCM-48/hydroxyapatite composites for drug delivery: Ibuprofen incorporation, location and release studies, *Mater. Sci. Eng., C*, 91, 734–742.

[31] dos Apostolos, R.C.R., Cipreste, M.F., de Sousa, R.G., and de Sousa, E.M.B., 2020, Multifunctional hybrid nanosystems based on mesoporous silica and hydroxyapatite nanoparticles applied as potential nanocarriers for theranostic applications, *J. Nanoparticle Res.*, 22 (12), 368.

[32] Windarti, T., Prasetya, N.B.A., Ngadiwiyana, N., and Nulandaya, L., 2023, Calcium phosphate cement composed of hydroxyapatite modified silica and polyeugenol as a bone filler material, *Indones. J. Chem.*, 23 (2), 499–509.

[33] Biglar, N., Chaychi Raghimi, E., Sadighian, S., Karamitanha, F., Zajkani, E., and Nourian, A., 2023, Effect of incorporating silica-hydroxyapatite-silver hybrid nanoparticles into the resin-modified glass ionomer on the adhesive remnant index score and shear bond strength of orthodontic metal brackets: An *in vitro* study, *Int. Orthod.*, 21 (3), 100761.

[34] Sumathra, M., Munusamy, M.A., Alarfaj, A.A., and Rajan, M., 2018, Osteoblast response to Vitamin D3 loaded cellulose enriched hydroxyapatite Mesoporous silica nanoparticles composite, *Biomed. Pharmacother.*, 103, 858–868.

[35] Reis, D.P., Filho, J.D.N., Rossi, A.L., de Almeida Neves, A., Portela, M.B., and da Silva, E.M., 2019, Remineralizing potential of dental composites containing silanized silica-hydroxyapatite (Si-HAp) nanoporous particles charged with sodium fluoride (NaF), *J. Dent.*, 90, 103211.

[36] Kuang, Z., Dai, G., Wan, R., Zhang, D., Zhao, C., Chen, C., Li, J., Gu, H., and Huang, W., 2021, Osteogenic and antibacterial dual functions of a novel levofloxacin loaded mesoporous silica microspheres/nano-hydroxyapatite/polyurethane composite scaffold, *Genes Dis.*, 8 (2),193–202.

[37] Wakily, H., Dabbagh, A., Abdullah, H., Abdul Halim, N.F., and Abu Kasim, N.H., 2015, Improved thermal and mechanical properties in hydroxyapatite-titanium composites by incorporating silica-coated titanium, *Mater. Lett.*, 143, 322–325.

[38] Ab Rahman, I., Ghazali, N.A.M. Wan Bakar, W.Z., and Masudi, S.M., 2017, Modification of glass ionomer cement by incorporating nanozirconia-hydroxyapatite-silica nano-powder composite by the one-pot technique for hardness and aesthetics improvement, *Ceram. Int.*, 43 (16), 13247–13253.

[39] Windarti, T., Nulandaya, L., Widjijono, W., and Nuryono, N., 2023, Synthesis and characterization of biphasic calcium phosphate substituted cerium as a potential osteoporotic bone filler, *Period. Polytech., Chem. Eng.*, 67 (2), 242–255.

[40] Palanisamy, G., Lee, J.H., and Lee, J., 2023, Curcumin-loaded hydroxyapatite nanoparticles for enriched removal of organic pollutants and inhibition of dual-species biofilm formation, *Environ. Technol. Innovation*, 32, 103364.

[41] Lee, W.H., Rohanizadeh, R., and Loo, C.Y., 2021, In situ functionalizing calcium phosphate biomaterials with curcumin for the prevention of bacterial biofilm infections, *Colloids Surf., B*, 206, 111938.

[42] de Deus, W.F., de França, B.M., Forero, J.S.B., Granato, A.E.C., Ulrich, H., Dória, A.C.O.C., Amaral, M.M., Slabon, A., and Rodrigues, B.V.M., 2021, Curcuminoid-tailored interfacial free energy of hydrophobic fibers for enhanced biological properties, *ACS Appl. Mater. Interfaces*, 13 (21), 24493–24504.

[43] Windarti, T., Widjijono, W., and Nuryono, N., 2021, Deposition of hydroxyapatite on silica made from rice husk ash to produce powder component of calcium phosphate cement, *Indones. J. Chem.*, 21 (3), 588–597.

[44] Sayed, M., Mahmoud, E.M., Saber, S.M., Raafat, S.N., Gomaa, S.M., and Naga, S.M., 2023, Effect of the injectable alginate/nano-hydroxyapatite and the silica/nano-hydroxyapatite composites on the stem cells: A comparative study, *J. Non-Cryst. Solids*, 610, 122327.

[45] Truite, C.V.R., Noronha, J.N.G., Prado, G.C., Santos, L.N., Palácios, R.S., Do Nascimento, A., Volnistem, E.A., da Silva Crozatti, T.T., Francisco, C.P., Sato, F., Weinand, W.R., Hernandes, L., and Matioli, G., 2022, Bioperformance studies of biphasic calcium phosphate scaffolds extracted from fish bones impregnated with free curcumin and complexed with β-cyclodextrin in bone regeneration, *Biomolecules*, 12 (3), 383.

[46] Shah, F.A., 2020, Characterization of synthetic hydroxyapatite fibers using high-resolution, polarized Raman spectroscopy, *Appl. Spectrosc.*, 75 (4), 475–479.

[47] Ramesh, G., Kaviyil, J.E., Paul, W., Sasi, R., and Joseph, R., 2022, Gallium-curcumin nanoparticle conjugates as an antibacterial agent against *Pseudomonas aeruginosa*: Synthesis and characterization, *ACS Omega*, 7 (8), 6795–6809.

[48] Sobeh, E.I., El-ghannam, G., Korany, R.M.S., Saleh, H.M., and Elfeky, S.A., 2022, Curcumin-loaded hydroxyapatite nanocomposite as a novel biocompatible shield for male Wistar rats from γ-irradiation hazard, *Chem.-Biol. Interact.*, 370, 110328.

[49] Yang, J., Chen, X., Wen, H., Chen, Y., Yu, Q., Shen, M., and Xie, J., 2022, Curcumin-loaded pH-sensitive biopolymer hydrogels: Fabrication, characterization, and release properties, *ACS Food Sci. Technol.*, 2 (3), 512–520.

[50] Van Nong, H., Hung, L.X., Thang, P.N., Chinh, V.D., Vu, L.V., Dung, P.T., Van Trung, T., and Nga, P.T., 2016, Fabrication and vibration characterization of curcumin extracted from turmeric (*Curcuma longa*) rhizomes of the northern Vietnam, *SpringerPlus*, 5, 1147.